RP Current Trends In Applied Sciences (e-ISSN: 2583-7486)
Vol. 5, No. 1 (January – March 2026) pp. 26–31

RESEARCH PLATEAU PUBLISHERS

Cite this article: S. Chowdhury, K. Ghosh, M. Gorai, P. Chandra, S.K. Mandal, Effect of Mn doping on the optical and dielectric properties of lead-free MABiCl perovskites, *RP Cur. Tr. Appl. Sci.* **5** (2026) 26–31.

Original Research Article

Effect of Mn doping on the optical and dielectric properties of lead-free MABiCl perovskites

Snigdha Chowdhury, Krishna Ghosh, Mou Gorai, Paramesh Chandra, Swapan K. Mandal

Department of Physics, Institute of Science, Visva-Bharati, Santiniketan 731235, India
*Corresponding author, E-mail: swapankumar.mandal@visva-bharati.ac.in

ARTICLE HISTORY
Received: 15 April 2026
Revised: 27 May 2026
Accepted: 27 May 2026
Published: 12 June 2026

KEYWORDS
AC conductivity;
Dielectric relaxation;
Impedance spectroscopy;
Lead-free perovskite;
Photoluminescence.

ABSTRACT
Lead-free halide perovskites have attracted significant attention as environmentally sustainable alternatives for optoelectronic applications, although optimizing the interplay between optical response and charge transport remains challenging. In this work, we address this issue through controlled 5% Mn doping in methylammonium bismuth chloride $(CH_3NH_3)_3Bi_2Cl_9$(MABiCl) perovskites at room temperature. UV–Vis spectroscopy reveals enhanced visible-light absorption in the 450–470 nm region accompanied by a slight bandgap reduction from 2.64 to 2.62 eV. Photoluminescence measurements show a pronounced emission band in the 540–560 nm region with increased intensity under 325 nm excitation after Mn incorporation, indicating an enhanced optical response. Dielectric measurements in the frequency range 50 Hz–5 MHz show a substantial increase in the low-frequency dielectric constant, indicating improved charge screening. Impedance and dielectric modulus analyses indicate reduced bulk resistance and faster relaxation behavior, while AC conductivity increases by nearly one order of magnitude from ~4×10^{-3} to ~1.3×10^{-2} $S.m^{-1}$. These results demonstrate that Mn doping is an effective strategy for improving the optical and dielectric performance of lead-free MABiCl perovskites.

1. Introduction

Metal organic halide perovskites particularly, with the general formula ABX_3-type structures (A = organic cation, B = metal cation, X = halide), have attracted significant attention as light-harvesting materials for photovoltaic and optoelectronic applications owing to their strong favorable charge-transport properties, strong optical absorption and low-cost solution processability [1–4]. Although lead-based perovskites have achieved remarkable power conversion efficiencies of up to 25.8%, concerns related to toxicity and long-term instability continue to hinder their large-scale commercialization [2]. Consequently, the development of stable and environmentally benign lead-free alternatives has become a major research focus. Among the potential substitutes, Bi^{3+} has emerged as a promising candidate because of its comparable electronic configuration to Pb^{2+} and its enhanced chemical stability. The bismuth-based compound $(CH_3NH_3)_3Bi_2Cl_9$(MABiCl) exhibits visible-light absorption and improved environmental compatibility partly due to the presence of stereochemically active $6s^2$ lone pair electrons [5, 6].

However, limited intrinsic charge-carrier density and relatively poor electrical conductivity restrict its broader functional applicability of MABiCl. Controlled doping has been widely explored as an effective strategy for tailoring the optoelectronic and electrical properties of halide perovskites to overcome these limitations. In the present work, Mn^{2+} doping was introduced into the MABiCl lattice to modulate its optical and dielectric characteristics. The incorporation of Mn is expected to influence defect states, polarization mechanisms, local lattice distortions and charge-transport behavior, thereby enhancing dielectric response and AC conductivity [7–9]. Therefore, a systematic investigation of MABiCl and Mn-doped MABiCl was carried out to understand the role of transition-metal doping in improving the optical and dielectric properties of lead-free bismuth-based perovskites.

2. Materials and methods

The starting materials used for the synthesis were methylamine (33 wt% in ethanol), hydrochloric acid (HCl, 35%, Merck Chemicals), bismuth chloride ($BiCl_3$, 99.99%, Sigma-Aldrich), manganese(II) chloride ($MnCl_2$, 99%, Merck Chemicals), anhydrous *N*,*N*-dimethylformamide (DMF, C_3H_7NO, 99.5%, Merck Chemicals) and absolute ethanol. All chemicals were of analytical grade and were used without further purification.

2.1 MABiCl Sample Preparation

The precursor methylammonium chloride (CH_3NH_3Cl, MACl) was prepared by reacting methylamine (33 wt% in ethanol) with hydrochloric acid (35%) in a 1:1 molar ratio in absolute ethanol under ice-bath conditions (0°C) for 2 h under constant stirring. The solvent was then evaporated under vacuum at 50°C for 24 h, yielding a white precipitate of MACl. The lead-free bismuth-based perovskite $CH_3NH_3)_3Bi_2Cl_9$ (MABiCl) was synthesized by dissolving CH_3NH_3Cl (5 mmol) and $BiCl_3$ (3.33 mmol) in DMF in a 3:2 molar ratio. The resulting solution was stirred at 50°C for 30 min until a homogeneous precursor solution was obtained. Subsequently, 20 mL of ethanol was added to induce precipitation of the product. The precipitate was filtered and dried under vacuum at

60°C to obtain the final MABiCl powder. The obtained powder was further dried at 40–50°C under ambient conditions prior to pellet preparation and electrical measurements.

2.2 5% Mn-doped MABiCl sample preparation

The 5% Mn-doped methylammonium bismuth chloride sample was synthesized using the same solution-based method. CH_3NH_3Cl (5 mmol, 0.3375 g) and $BiCl_3$ were used in a 3:2 molar ratio, with partial substitution of the Bi precursor by $MnCl_2$ corresponding to 5% Mn doping. The calculated amounts of CH_3NH_3Cl, $BiCl_3$, and $MnCl_2$ were dissolved in DMF and stirred at 50°C for 30 min to obtain a homogeneous precursor solution. Then, 20 mL of ethanol was added to induce precipitation. The resulting precipitate was filtered and dried under vacuum at 60 °C to obtain the Mn-doped powder. The powder was further dried at 40–50°C under ambient conditions prior to pellet preparation and electrical measurements.

3. Material characterization

Scanning electron microscopy (SEM, ZEISS Gemini SEM 450) was employed to examine the surface morphology of the pristine and Mn-doped samples. UV–Visible absorption spectra were recorded using a custom-built spectroscopic setup in the wavelength range of 400–600 nm. The optical bandgap values were estimated from Tauc plots of $(\alpha h\nu)^2$ vs. $h\nu$. Photoluminescence (PL) spectra were recorded at room temperature using a photoluminescence spectrometer under an excitation wavelength of 325 nm. For dielectric and impedance measurements, the prepared powders were pelletized using a hydraulic pellet press under an applied pressure of approximately 5 ton for 5 min. The pellets had a diameter of 5 mm and a thickness of approximately 1 mm. Thin silver paste electrodes were applied on both sides of each pellet to ensure good electrical contact. The electrical measurements were carried out on pelletized samples of pristine MABiCl and 5% Mn-doped MABiCl using a Hioki LCR-3570 LCR meter at room temperature over the frequency range of 50 Hz to 5 MHz.

4. Results and discussion

4.1 FESEM analysis

Figure 1 (a), (b) shows the morphological structure of MABiCl and 5% Mn-doped MABiCl respectively. Both samples exhibit flake-like and plate-shaped microstructures with lateral dimensions of approximately 200 nm. The MABiCl sample shows densely jumbled grains with a relatively compact morphology. After Mn addition larger and more distinct flake-like features are observed along with improved grain connectivity and increased surface roughness. These morphological changes suggest that Mn doping influences the nucleation and crystal growth process; that's why we can get improved charge transport behavior.

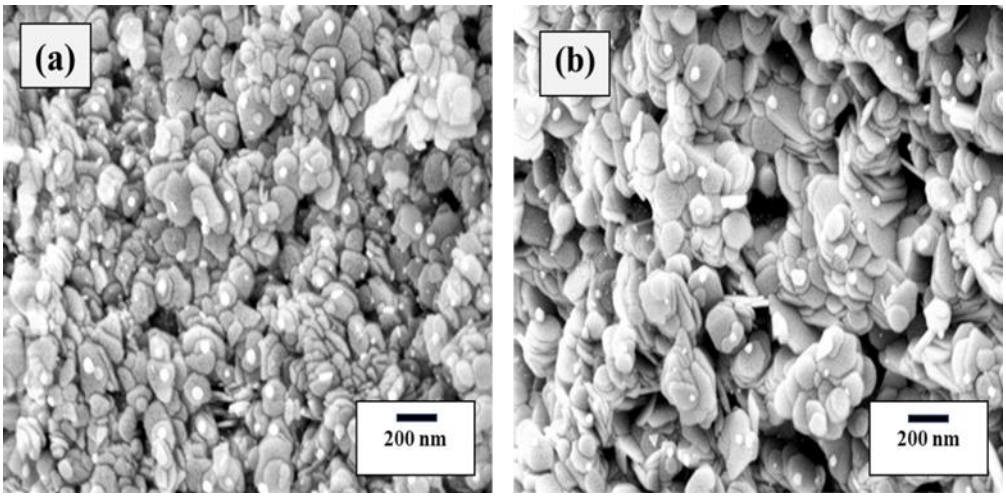

Figure 1: FESEM images of (a) MABiCl and (b) 5% Mn-doped MABiCl showing flake-like morphology and changes in grain distribution after Mn doping.

4.2 Optical studies

The UV–Vis absorption spectra of undoped MABiCl and 5% Mn-doped MABiCl are shown in Figure 2(a). Both samples exhibit significant absorption in the visible region around 450–470 nm [10, 11]. The Mn-doped sample shows enhanced absorbance compared to the undoped sample which indicates Mn incorporation modifies the optical response of the host lattice. This enhancement may be associated with Mn-induced changes in the electronic structure and the introduction of defect-assisted absorption state results. The optical bandgap was estimated from Tauc plots of $(\alpha h\nu)^2$vs. $h\nu$ as shown in Figure 2(b). A slight bandgap reduction from 2.64 eV for the undoped sample to 2.62 eV for the Mn-doped sample was observed [5, 12]. This small bandgap narrowing suggests that Mn incorporation may introduce localized impurity levels or induce local lattice distortion, thereby promoting optical transitions.

Photoluminescence (PL) spectra recorded at room temperature are presented in Figure 2(c). Both samples exhibit a broad emission band in the 540–560 nm region. The Mn-doped sample shows higher PL intensity than the undoped sample indicating enhanced radiative recombination and stronger interaction of charge carriers with luminescent centers [12]. These observations suggest that Mn doping effectively modifies the optical excitation and recombination behavior of MABiCl which can be advantageous for optoelectronic applications.

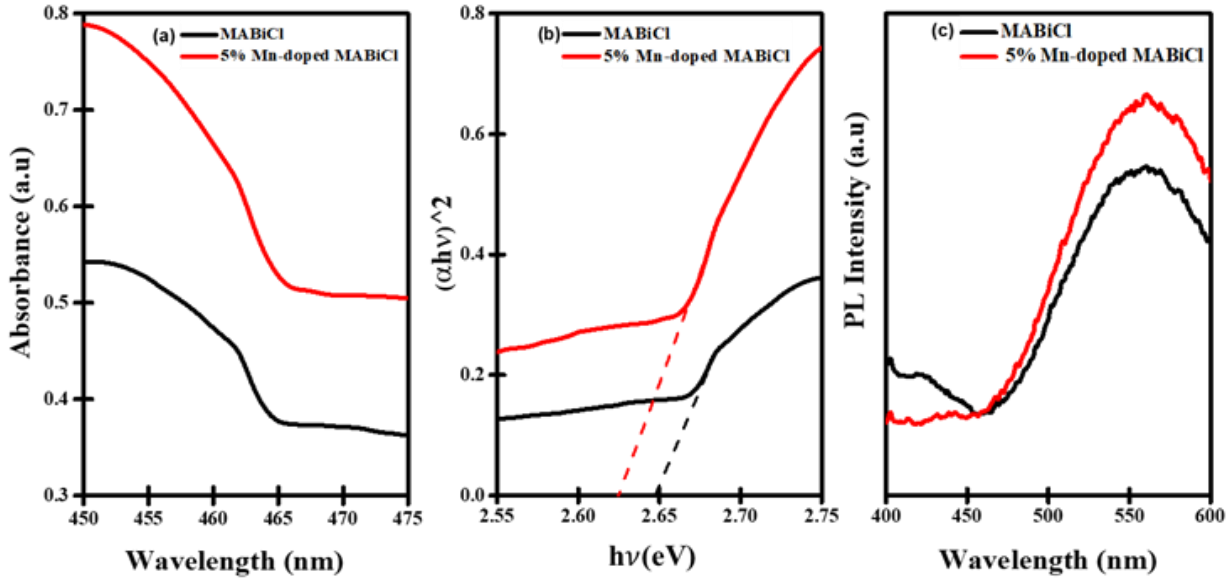

Figure 2: (a) Optical absorption spectra (b) Corresponding *Tauc* plot showing enhanced absorption and slight bandgap narrowing after Mn doping (c) Photoluminescence (PL) spectra of MABiCl and 5% Mn-doped MABiCl showing enhanced emission intensity after Mn doping.

4.3 Impedance spectroscopy

The complex impedance spectra of MABiCl and 5% Mn-doped MABiCl were analyzed at room temperature over the frequency (ω) range 50 Hz to 5 MHz to investigate their electrical transport behavior. The real part of impedance (Z') exhibits high values at low frequencies and with increasing frequency impedance decreases, as shown in Figure 3(a). For the MABiCl sample, Z' decreases from ~1.0 × 10^5 Ω at low frequency (~10^2 Hz) to ~3 × 10^2 Ω at high frequency (~10^6 Hz). This behavior is commonly ascribed to electrode polarization and limited charge carrier mobility. These effects diminish at higher frequencies which leads to a decrease in impedance [5, 13].

Across the entire measured frequency range, the Mn-doped sample exhibits lower Z' with a value of ~4 × 10^4 Ω at low frequency. This reduction in impedance indicates improved electrical conductivity after Mn doping and enhanced charge-carrier transport within the lattice [14]. The imaginary impedance (Z'') exhibits a relaxation peak for both samples. The undoped sample exhibits a relatively sharper peak centered around (~4 × 10^4 Ω) whereas the Mn-doped sample exhibits a broader peak at a lower frequency (~6 × 10^3 Hz) with a lower magnitude (~1.2 × 10^4 Ω). The broadening of the peak in the Mn-doped sample indicates a distribution of relaxation times and suggests non-Debye-type relaxation behavior. The Nyquist plots display a single depressed semicircle for both samples corresponding predominantly to the bulk response of the material which is shown in Figure 3(c). The bulk resistance decreases from approximately ~9.8 × 10^4 Ω for undoped MABiCl to ~5 × 10^4 Ω for the Mn-doped sample. The depressed nature of the semicircle further supports non-Debye relaxation behavior.

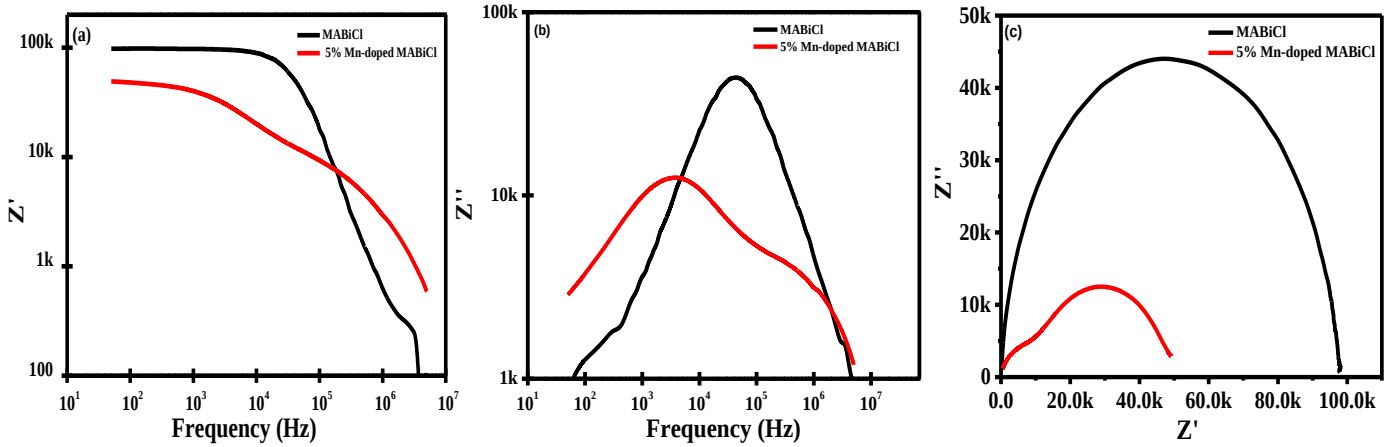

Figure 3: Impedance spectroscopy of MABiCl and 5% Mn-doped MABiCl (a) real part of impedance vs. frequency, (b) imaginary part of impedance vs. frequency, and (c) Nyquist plot.

4.4 Dielectric permittivity

The dielectric response of MABiCl and 5% Mn-doped MABiCl was analyzed in terms of the complex permittivity, which is expressed as:

$$\varepsilon(\omega) = \varepsilon'(\omega) - j\varepsilon''(\omega) \quad (1)$$

where $\varepsilon'(\omega)$represents the dielectric constant and $\varepsilon''(\omega)$ represents the dielectric loss [8–10]. These quantities were calculated from the impedance data using

$$\varepsilon'(\omega) = \frac{Z''}{\omega C_0 (Z'^2 + Z''^2)} \quad (2)$$

$$\varepsilon''(\omega) = \frac{Z'}{\omega C_0 (Z'^2 + Z''^2)} \quad (3)$$

where $\omega = 2\pi f$ is angular frequency and $C_0 = \varepsilon_0 \frac{A}{t}$, with ε_0 being the permittivity of free space, A is the cross-sectional area and t the thickness of the pellet. The frequency dependence of ε' and $\varepsilon''$is shown in Figure 4. Both samples display strong dielectric dispersion with high permittivity at low frequencies followed by a gradual decrease with increasing frequency. This behavior can be explained using Koop's phenomenological theory based on the Maxwell–Wagner interfacial polarization model, in which the material is considered to consist of semiconducting grains separated by more resistive grain boundaries [15, 16]. At low frequencies charge accumulation at grain boundaries causes strong interfacial polarization resulting in higher dielectric constant values. Ionic polarization from methylammonium and bismuth-halide charge centers may also contribute. As frequency increases, charge carriers cannot follow the rapidly alternating field leading to reduced polarization and a lower dielectric constant.

At low frequencies the Mn-doped sample demonstrates a dielectric constant nearly one order of magnitude higher than that of the undoped sample reflecting enhanced polarization and charge-storage capability. This enhancement may be associated with increased hopping sites and modification of grain-boundary interfaces introduced by Mn doping [17]. Moreover, the Mn-doped sample maintains higher dielectric loss across the measured frequency range, as shown in Figure 4(b). This can happen for increased energy dissipation due to polarization processes [18].

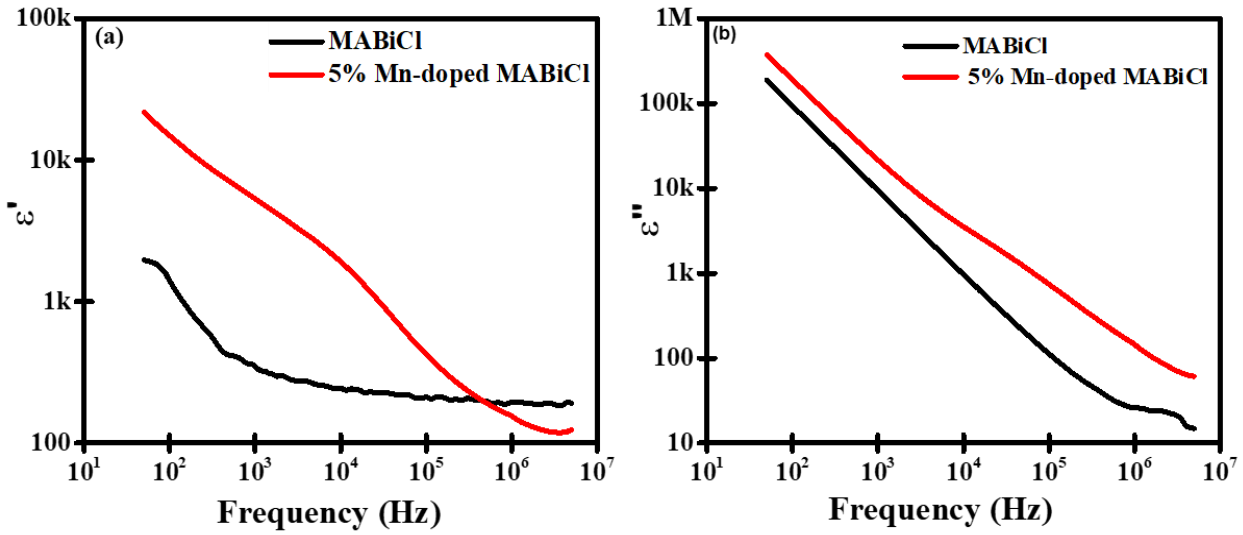

Figure 4: Frequency-dependent variation of (a) dielectric constant $\varepsilon'$and (b) dielectric loss ε'' for MABiCl and 5% Mn-doped MABiCl.

4.5 Dielectric modulus

The electric modulus formalism is a useful approach for analyzing dielectric relaxation behavior and minimizing the influence of electrode polarization in dielectric measurements.

$$M(\omega) = M'(\omega) + j\, M''(\omega) = \frac{1}{\varepsilon(\omega)} = \frac{\varepsilon'(\omega)}{(\varepsilon'^2 + \varepsilon''^2)} + j\frac{\varepsilon''(\omega)}{(\varepsilon'^2 + \varepsilon''^2)} \quad (4)$$

The variation of $M'$and $M''$with frequency is shown in Figure 5. The real part (M') remains very small in the low-frequency region ($\sim 10^{-7}$–10^{-6}), which can be possible for the suppression of electrode polarization and the dominance of long-range charge-carrier motion. With increasing frequency M'gradually increases and approaches a nearly constant value at high frequency ($\sim 10^{-3}$Hz) reflecting a transition from long-range mobility to localized dielectric relaxation. The Mn-doped sample exhibits a comparatively more gradual increase in M', Mn doping modifies the relaxation dynamics of the host lattice [19]. The imaginary part (M'') shown in Figure.6(b), display a distinct relaxation peak for both samples. The undoped samples shows a peak around 4×10^4– 6×10^4 Hz with a magnitude of approximately 2×10^{-3} whereas the Mn-doped sample shows a broader peak shifted toward higher frequency ($\sim 10^6$ Hz) with a slightly larger magnitude ($\sim 3 \times 10^{-3}$). The shift of the relaxation peak toward higher frequency indicates a decrease in relaxation time in the Mn-doped sample [20]. Furthermore, the asymmetric broadening of the M''peak suggests a distribution of relaxation times consistent with non-Debye relaxation behavior. Mn incorporation significantly affects the electrical relaxation dynamics and contributes to improved charge transport in MABiCl [21].

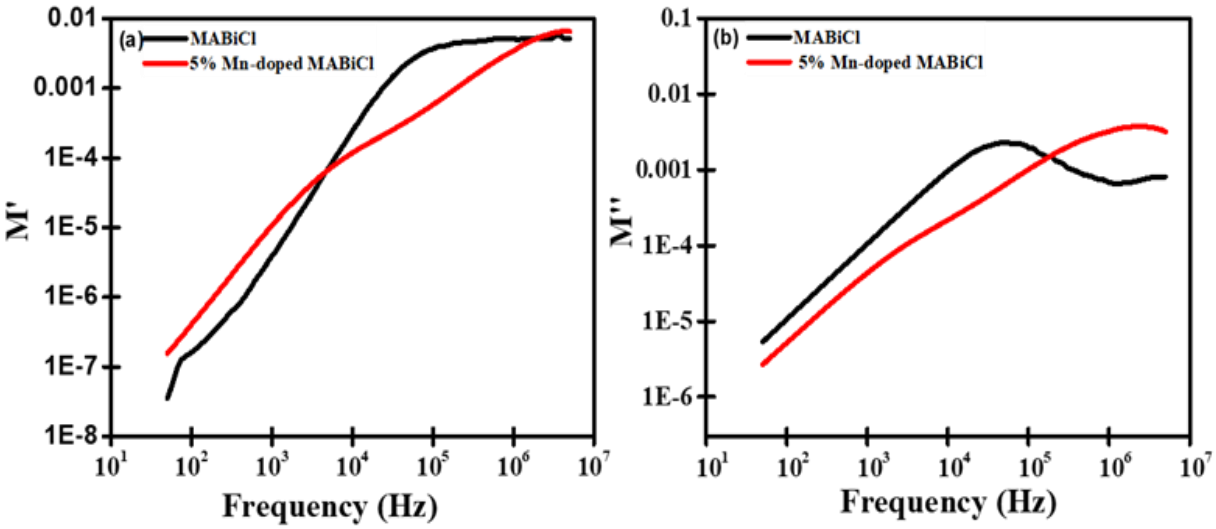

Figure 5: Dielectric modulus spectra showing (a) $M'$and (b) $M''$for MABiCl and 5% Mn-doped MABiCl.

4.6 AC conductivity

The frequency dependence of AC conductivity (σ_{ac}) for MABiCl and 5% Mn-doped MABiCl is shown in Figure 6. over the frequency range 50 Hz to 5 MHz. AC conductivity is a useful parameter for understanding charge transport and dielectric relaxation processes in halide perovskites. The observed conductivity behavior follows Jonscher's universal power law:

$$\sigma(\omega)=\sigma_{dc}+A\omega^{n} \quad (5)$$

where σ_{dc} is the dc conductivity, A is a constant and n is the frequency exponent ($0 < n < 1$). Both samples exhibit a nearly constant conductivity at low frequencies, which corresponds to the DC conductivity region and indicates long-range movement of charge carriers. The conductivity increases for both samples as frequency gradually rises. This behavior's possible reason can be the conduction mechanism changes from long range transport at low frequencies to localized hopping conduction at higher frequencies. The Mn-doped sample exhibits higher conductivity than the undoped sample throughout the measured frequency range. At high frequencies, the conductivity reaches approximately 1.3×10^{-2} S.m^{-1} for the Mn-doped sample compared with $\sim 4 \times 10^{-3}$ S.m^{-1} for the undoped sample. These observations are consistent with the impedance results, which also indicate reduced resistance and improved electrical transport after Mn doping [22–24]. The frequency exponent (n) obtained from log σ vs log f plots for the undoped sample its value is 0.52, while the 5% Mn-doped sample shows a lower value of 0.28. The undoped sample suggests a correlated barrier hopping (CBH) mechanism, where charge carriers hop between localized states over potential barriers. After Mn doping, the n value decreases to 0.28, indicating a transition toward long-range hopping conduction with stronger interaction between charge carriers and localized states [25].

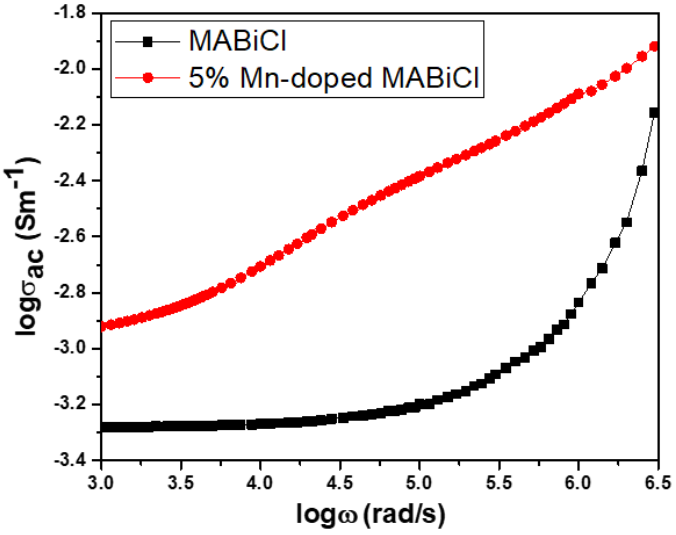

Figure 6: Frequency-dependent AC conductivity of MABiCl and 5% Mn-doped MABiCl samples at room temperature.

5. Conclusions

In summary, Mn doping effectively improves the optical and dielectric properties of lead-free $(CH_3NH_3)_3Bi_2Cl_9$ perovskite. The Mn-doped sample exhibits enhanced visible-light absorption, slight bandgap narrowing, and stronger photoluminescence emission, indicating an improved optical response. Electrical investigations further reveal reduced bulk resistance, enhanced dielectric permittivity, modified

relaxation behavior, and a significant increase in AC conductivity, consistent with improved charge-carrier transport through hopping-assisted mechanisms. These results demonstrate that Mn incorporation is an effective approach for tuning both the optical and electrical characteristics of $(CH_3NH_3)_3Bi_2Cl_9$, thereby enhancing its potential for lead-free optoelectronic and energy-related applications. Overall, the present study highlights transition-metal doping as a promising route for improving the multifunctional performance of bismuth-based halide perovskites.

Authors' contributions

The author read and approved the final manuscript.

Conflicts of interest

The author declares no conflict of interest.

Funding

SKM received funding from CSIR, India (Scheme No. 03/1489/2023/EMR-II).

Data availability

No new data were created.

References

[1] H. Slavney, T. Hu, A. M. Lindenberg, H. I. Karunadasa, A bismuth-halide double perovskite with long carrier recombination lifetime for photovoltaic applications, *J. Am. Chem. Soc.* **138** (2016) 2138–2141.

[2] G. E. Eperon, S. D. Stranks, C. Menelaou, M. B. Johnston, L. M. Herz, H. J. Snaith, Formamidinium lead trihalide: a broadly tunable perovskite for efficient planar heterojunction solar cells, *Energy & Environmental Science* **7** (2014) 982–988.

[3] J.M. Azpiroz, E. Mosconi, J. Bisquert, F. De Angelis, Defect migration in methylammonium lead iodide and its role in perovskite solar cell operation, *Energy Environ. Sci.* **8** (2015) 2118–2127.

[4] M. Saliba, T. Matsui, K. Domanski, J.-Y. Seo, A. Ummadisingu, S. M. Zakeeruddin, J.-P. Correa-Baena, W. R. Tress, A. Abate, A. Hagfeldt, M. Grätzel, Incorporation of rubidium cations into perovskite solar cells improves photovoltaic performance, *Science* **354** (2016) 206–209.

[5] P. Chandra, S.K. Mandal, Electrical and dielectric properties of perovskite materials, *Phys. B: Condens. Matter* **625** (2022) 413536.

[6] B.W. Park, B. Philippe, X. Zhang, H. Rensmo, G. Boschloo, E.M.J. Johansson, Bismuth based hybrid perovskites for optoelectronic applications, *Adv. Mater.* **27** (2015) 6806–6813.

[7] B. Harihara-Venkataraman, K.B.R. Varma, Ionic conductivity and dielectric behaviour of ceramic materials, *Solid State Ionics* **167** (2004) 197–202.

[8] P. Chandra, S. Saha, S.K. Mandal, Frequency and temperature-dependent dielectric characteristics of lead-free Br-doped perovskites $(CH_3NH_3)_3Bi_2Cl_9$ and $(CH_3NH_3)_3Bi_xCl_{9-x}$, *Mater. Today Proc.* **66** (2022) 3302–3306.

[9] R. Kaur, V. Sharma, M. Kumar, M. Singh, A. Singh, Structural and dielectric properties of alloy compounds *J. Alloys Compd.* **735** (2018) 1472–1478.

[10] A. Kojima, K. Teshima, Y. Shirai, T. Miyasaka, Organometal halide perovskites as visible-light sensitizers for photovoltaic cells, *J. Am. Chem. Soc.* **131** (2009) 6050–6051.

[11] K. Ahmad, S.N. Ansari, K. Natarajan, S.M. Mobin, Design and synthesis of 1D-polymeric chain based $[(CH_3NH_3)_3Bi_2Cl_9]_n$ perovskite: a new light absorber material for lead-free perovskite solar cells, *ACS Appl. Energy Mater.* **1** (2018) 2405–2409.

[12] W. Liu, Q. Lin, H. Li, K. Wu, I. Robel, J. M. Pietryga, V. I. Klimov, Mn^{2+}-doped lead halide perovskite nanocrystals with dual-color emission controlled by halide content, *Adv. Mater.* **28** (2016) 1120–1125.

[13] Cole, Kenneth S., and Robert H. Cole. "Dispersion and absorption in dielectrics I. Alternating current characteristics." *The Journal of chemical physics* 9.4 (1941): 341-351.

[14] Ch. Rayssi, S. El Kossi, J. Dhahri, K. Khirouni, Frequency and temperature-dependent dielectric permittivity and electric modulus studies of $Ca_{0.85}Er_{0.1}Ti_{1-x}Co_{4x/3}O_3$ solid solution, *RSC Adv.* **8** (2018) 17139–17150.

[15] Wasylishen, Roderick E., Osvald Knop, and J. Bruce Macdonald. "Cation rotation in methylammonium lead halides." *Solid state communications* 56.7 (1985): 581-582.

[16] T. Prodromakis, C.J.A.S.S. Papavassiliou, Engineering the Maxwell–Wagner polarization effect, *Appl. Surf. Sci.* **255** (2009) 6989–6994.

[17] M.S. Sheikh, A.P. Sakhya, P. Sadhukhan, A. Dutta, S.Das, T.P. Sinha, Dielectric and electrical properties of ferroelectric materials, *Ferroelectrics* **514** (2017) 146–152.

[18] H. Belmabrouk, T. Alharbi, Dielectric properties and conduction mechanism of $La_{0.7}Sr_{0.25}Na_{0.05}Mn_{0.95}Al_{0.05}O_3$ perovskite manganite, *J. Taibah Univ. Sci.* **17** (2023) 2204809.

[19] L. Sahoo, S. Mohanty, S. K. Rout, P. Nayak, Impedance spectroscopy and optical properties of lanthanum-modified Bi_2FeMnO_6 for NTC thermistor applications, *Mater. Adv.* **6**(2025) 1455–1467.

[20] A. Choudhary, R. Kumar, A. Kumar, Structural, dielectric and energy storage characteristics of $(Pb_{1-x}Sr_x)(Zr_{0.80}Ti_{0.20})O_3$ antiferroelectric compositions, *J. Alloys Compd.* **899** (2022) 163395.

[21] A.K. Jonscher, Dielectric relaxation in solids, *J. Phys. D: Appl. Phys.* **32** (1999) R57–R70.

[22] A. Ghosh, Frequency-dependent conductivity in bismuth vanadate glassy semiconductors, *Phys. Rev. B* **41** (1990) 1479.

[23] J.C. Dyre, The random free-energy barrier model for ac conduction in disordered solids, J. Appl. Phys. 64 (1988) 2456-2468.

[24] K. Funke, Jump relaxation in solid electrolytes, *Prog. Solid State Chem.* **22** (1993) 111-195.

[25] Mahato, D. K., Dutta, A., & Sinha, T. P. Impedance spectroscopy analysis of double perovskite Ho_2NiTiO_6. Journal of Materials Science, **45**, 6757–6762 (2010).